Journal of Alloys and Compounds 851 (2021) 156936

Contents lists available at ScienceDirect

Journal of Alloys and Compounds

journal homepage: http://www.elsevier.com/locate/jalcom

Resistive switching and multiferroic behavior of $La_{0.5}Pr_{0.5}FeO_3$ ferrite thin films

M.G.A. Ranieri [a, b], P.P. Ortega [c, *], H. Moreno [c], M.A. Ramirez [c], E.C. Aguiar [d], A.Z. Simões [c]

[a] São Paulo State University (UNESP), Chemistry Institute, Araraquara, São Paulo, Brazil
[b] Federal University of Itajubá (UNIFEI), Physics and Chemistry Institute, Itajubá, Minas Gerais, Brazil
[c] São Paulo State University (UNESP), School of Engineering of Guaratinguetá, Guaratinguetá, São Paulo, Brazil
[d] State University of Mato Grosso do Sul (UEMS), Materials Research Center, Dourados, Mato Grosso do Sul, Brazil

ARTICLE INFO

Article history:
Received 30 March 2020
Received in revised form
16 August 2020
Accepted 28 August 2020
Available online 29 August 2020

Keywords:
$La_{0.5}Pr_{0.5}FeO_3$
Thin films
Resistive switching
Magnetic response

ABSTRACT

This study examines resistive switching behavior and magnetoelectric coupling in $La_{0.5}Pr_{0.5}FeO_3$ thin films obtained through the polymeric precursor method at a temperature of 500 °C for 2 h. The real and imaginary part of dielectric constant (ε' and ε'') as a function of temperature demonstrate significant values with increasing temperature and can be caused by the ferroelectric ordering in the present system. The magnetic and dielectric measurements suggest a coupling between magnetic and electric dipoles at room temperature. The magnetization versus temperature curves under zero-field cooling (ZFC) and field cooling (FC) conditions suggest antiferromagnetic to ferromagnetic transition. The maximum magnetoelectric coupling value is ~0.06 for H ~1.7 T. By varying the applied electric field, we noted the resistive memory phenomenon from current-voltage (I–V) characteristics being reversibly switched between two stable resistance states. Such behavior can be ascribed to the electron hopping from Fe^{2+} to Fe^{3+} levels with oxygen vacancies present in the lattice, as evidenced using XPS analysis. These state-of-art analyses motivated us to study the introduction of praseodymium (Pr) in La^{3+} sites, considering that $LaFeO_3$ shows paramagnetic behavior at room temperature. $La_{0.5}Pr_{0.5}FeO_3$ thin films exhibited slightly ferromagnetic behavior associated with coupling between cations at the octahedral and tetrahedral sites with the coexistence of resistive switching and magnetoelectric coupling behavior.

1. Introduction

Multiferroics display more than one ferroic ordering (ferromagnetism, ferroelectricity, and ferroelasticity) simultaneously in a single-phase compound [1,2]. In such materials, the coupling between ferromagnetism and ferroelectricity – known as the magnetoelectric effect – makes it possible to control electric polarization through an applied magnetic field and vice versa, enabling auspicious applications in the field of spintronics, information storage devices, magnetoelectric sensors and energy conversion [1–4]. However, there are few multiferroics which exhibit magnetoelectric coupling at room temperature [5] since the requirements for ferromagnetism and ferroelectricity are antagonistic. The electric polarization in ferroelectric perovskite oxides arises from the cation off-centering associated with empty d-shells (e.g. Ti^{4+} has an empty d-shell in $BaTiO_3$). On the other hand, magnetism results from unpaired electrons in a partially filled d-shell, as seen with Fe, Cr, and Mn transition metals [6,7]. Therefore, as the conditions for magnetic and electric moments to coexist are mutually exclusive, alternatives to induce magnetism (electrons in an f-shell, for example) and ferroelectricity in a single-phase compound at room temperature is a holy grail pursued by materials scientists.

To overcome such obstacles, $LaFeO_3$ (LFO) – a perovskite oxide belonging to the rare-earth orthoferrite family – emerges as a multiferroic material exhibiting both antiferromagnetic and ferroelectric orderings [8]. It belongs to an orthorhombic perovskite structure with a Pbnm space group [9]. The ferroelectric ordering of LFO originates from a local electric field induced by the lattice distortion, while the magnetic ordering originates from 3d electrons present in the transition metal ions [1,10,11]. Recent theoretical studies have highlighted the importance of biquadratic couplings on the properties of multiferroic AMO_3 compounds, such as rotomagnetic coupling between the antiferromagnetic (AFM)

* Corresponding author.
E-mail address: pedro.ortega@unesp.br (P.P. Ortega).

https://doi.org/10.1016/j.jallcom.2020.156936
0925-8388/

order and oxygen octahedra (MO_6) tilts in antiferrodistorted (AFD) perovskites. This coupling may be related to the dependence of the exchange interaction on the bond angle between magnetic and nonmagnetic ions. The AFD-AFM rotomagnetic coupling exercises significant influence on the magnetic and dielectric permittivity, order parameters, as well as on the AFM and AFD transition temperatures, as demonstrated by Eliseev et al. [12] and Morozovska et al. [13]. Moreover, a study performed by Karpinsky et al. [14] has shown that rotomagnetic AFD-AFM coupling on pure and La-doped $BiFeO_3$ is very important to describe its ferroelectric polarization, AFD tilt behavior, as well as the temperature stability of the antiferromagnetic, ferroelectric, and antiferrodistortive phases.

Despite its multiferroic nature, LFO shows weak magnetic and ferroelectric polarization [11]. Hence, to improve magnetoelectric coupling of LFO, the introduction of praseodymium (Pr) in La^{3+} sites is a promising alternative to reach the coupling between the electric and magnetic polarization states of the antiferromagnetic (AFM) layers. Such layers secure an adjacent ferromagnetic (FM) layer by force of the exchange-bias coupling [15,16].

Noel et al. [17] have proposed a new type of spintronics employed in spin field-effect transistors and spin Hall transistors, in which non-volatility would not originate from ferromagnetism but rather, from ferroelectricity. In their study, the authors deposited NiFe and Al films using d.c. magnetron sputtering on TiO_2-terminated (001)-oriented STO substrates. Such an effect suggests the presence of a switchable polarization with associated polar displacements of cations and anions affecting the band structure. The two-dimensional electron gas allows the manipulation of the spin-orbit properties and efficiently convert**s** spin currents into positive or negative charge currents, depending on the polarization direction.

In another study, Mundy et al. [18] synthesized superlattices of $(LuFeO_3)_9/(LuFe_2O_4)_1$ by reactive-oxide molecular-beam epitaxy. The authors demonstrated the magnetoelectric coupling of the ferroelectric polarization to the co-linear ferrimagnetic order at 200 K. Such coupling is probably distinct from the more extensively studied Dzyaloshinskii–Moriya coupling, which was previously observed as between ferroelectricity and weakly canted antiferromagnetism at room temperature in $BiFeO_3$.

Recently, our group has put much effort into characterizing the electrical properties of $La_{0.5}Sm_{0.5}FeO_3$ thin films obtained by the polymeric precursor method [19]. Due to the loss of oxygen during sintering, samarium (Sm) substitution in the antiferromagnetic insulator ($LaFeO_3$) leads to a semiconductor state. The resistivity dependence of temperature measurements demonstrated that a low resistivity semiconducting material was attained. The grains and grain boundaries observed in the Nyquist diagram reveal different resistivity values caused by oxygen vacancies, which are in equilibrium in the system. Doping the orthoferrite with rare-earth elements leads to the creation of oxygen vacancies to maintain electric neutrality. Therefore, such positive mobile charges can move through the sample under high electric fields to keep thermodynamic equilibrium and agglomerate around the surface, thus causing negative ion polarization. Consequently, the donor oxygen and receiver lanthanum ions become locally unbalanced, turning the surface into an n-type transporter and the area near the electrode into a p-type. The application of an electric field in the opposite direction of the oxygen vacancies flux makes them migrate to these gaps, becoming an electronic insulator. However, a weak ferroelectric mode is observed from the capacitance-voltage (C–V) plot at room temperature.

The magnetic and ferroelectric properties of the $La_{0.5}Pr_{0.5}FeO_3$ films were explored due to their significant potential and use in electronic device engineering applications. In a recent study [20], we have shown that nano grained LFO thin films obtained by the chemical method proposed in the present research presented a coercive magnetic field at room temperature and p-type conduction. Moreover, strong magnetization was observed, which is an indication of uncompensated magnetic moments of Fe^{3+}. Therefore, the main goal of this study is possible induction of the FM (FE) phase in $La_{0.5}Pr_{0.5}FeO_3$ thin films through the application of an electric (magnetic) field due to the ME coupling. Moreover, the study seeks to comprehend the resistive switching behavior of the orthoferrite perovskite structure with applications in next-generation memory devices, considering that $LaFeO_3$ without Pr in the composition shows paramagnetic behavior at room temperature.

2. Experimental procedure

The $La_{0.5}Pr_{0.5}FeO_3$ thin film was prepared using the polymeric precursor method (PPM), as described in a previous study [21]. First, the raw lanthanum precursors (La_2O_3 - J.T.Baker 99.5%), praseodymium (Pr_2O_3 - Aldrich 99.9%), and iron ($Fe(NH_4)_2H(C_6H_5O_7)_2$ - Vetec 99.9%) were dissolved in water. Then, ethylene glycol ($C_2H_6O_2$ - Aldrich 99.5%) and a concentrated solution of citric acid ($C_6H_8O_7 \cdot H_2O$ - Merck 99.5%) were added to each solution under constant heating and stirring with a metal to citric acid to ethylene glycol molar ratio of 1:4:16, respectively. The three solutions (La, Fe, and Pr) were then mixed using constant stirring at 90 °C. Using a Brookfield viscometer, the viscosity was set at 20 cP by adjusting the water content. The spin-coating technique was used to deposit the solution onto the Pt(111)/Ti/SiO_2/Si substrate's surface at 5000 rpm for 30 s. Each layer was annealed at 300 °C for 1 h with a slow heating rate (3 °C/min) and crystallized at 500 °C for 2 h in a conventional furnace. After ten layers were deposited, the multilayered LFO: Pr thin films were obtained. The number of layers was optimized to reach the thickness needed to achieve the electrical properties. Three films were prepared for the test devices. On the 1 cm × 1 cm film, several gold electrodes (diameter ~ 0.5 mm) were sputtered using shadow mask. The polar properties of the multiferroic film were measured in the center film in order to guarantee reproducibility and repeatability of the obtained properties. Three samples were prepared: sample 1 was used for XRD, Raman, FEG-SEM and XPS analyses, while samples 2 and 3 were reserved for electrical measurements. The P-E, M-H and I–V curves were measured at room temperature. However, cool-downs on the same sample for zero-field cooling (ZFC) and field cooling (FC) measurements were also performed. After conducting a first cool-down at low temperature, it is possible to recover the initial state by heating the sample to room temperature. P–H loop (measured on sample 2) revealed that the remnant ferroelectric state is not lost after heating, thus showing a lower and positive spin signal. This is consistent with our observation of a voltage-induced ferroelectricity at low temperature. For dielectric measurements, sample 3 was heated from room temperature to 260 °C. The high values for real and imaginary part of dielectric constant (ε' and ε'') is indicative of ferroelectric ordering in the present system, thus enabling a return of the hysteretic behavior and the remanence of the polarization.

The thin films were characterized by X-ray diffraction (XRD) using Cu-Kα radiation in the 2θ range between 20 and 60° (Rigaku-DMax 2000 PC). Scherrer's equation ($d = k\lambda/\beta\cos\theta$) was used to calculate the crystallite size (d), where k is a constant, λ is the Cu-Kα radiation wavelength of the main peak, and β and θ are the full width at half maximum (FWHM) and the diffraction angle of the main peak, respectively. The crystalline structure of the films was refined on the software Topas V5 [22] using the Rietveld method [23]. Raman spectroscopy (LabRAM iHR550 Horiba Jobin Yvon) was performed with a 514 nm wavelength laser as the excitation source

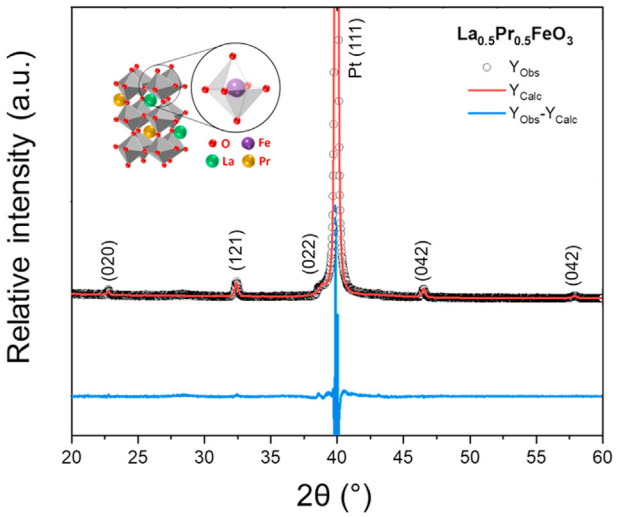

Fig. 1. X-ray diffraction pattern of the $La_{0.5}Pr_{0.5}FeO_3$ thin films deposited on Pt/Ti/SiO_2/Si(100) substrates and annealed at 500 °C for 2 h.

and spectral resolution of 1 cm^{-1} with 40 scans, from 100 to 800 cm^{-1}, coupled to a CCD detector. The thickness of the films was obtained by scanning electron microscopy (SEM) on a Topcom SM-300 equipment using backscattered electrons to generate the transversal section image. XPS analysis was carried out to verify modifications in the chemical composition on the surface of the treated specimens. The XPS measurements were performed at a pressure lesser than 10^{-7} Pa using a commercial spectrometer (UNI-SPECS UHV). The Mg K line was used (h = 1253.6 eV), and the analyzer pass energy was set to 10 eV. The inelastic background of the Fe 2p and O 1s electron core-level spectra were subtracted using Shirley's method.

To perform the electrical measurements, a top gold electrode (diameter ~ 0.5 mm) was sputtered through a shadow mask at room temperature and heat-treated in an oxygen atmosphere at 300 °C for 1 h, forming an Au/LFO: Pr/Pt/Ti/SiO_2/Si capacitor. Analysis of the capacitor's electrical properties was carried out on a Radiant Technology RT6000 A tester. Characteristic current-voltage (I–V) curves were obtained at room temperature with voltage sweep from −40 V to 0, 0 to +40 V, +40 V to 0, and 0 to −40 V and current compliance limited to 1.0 μA. The curves were traced using 0.1 V paces and a time of 1.0 s to each voltage. The real (ε') and imaginary (ε'') parts of the dielectric constant were measured from 25 °C to 280 °C at frequencies from 0.001 to 1000 kHz, using impedance equipment (HP 4192A).

Ferroelectricity of the thin films was evaluated using a Sawyer-Tower circuit attached to a computer-controlled standardized ferroelectric test system. The hysteresis curves – magnetization vs. the applied magnetic field (M-H) – data along with field cooled (FC) and zero-field-cooled (ZFC) magnetizations as a function of temperature were recorded using a SQUID magnetometer (MPMS XL 7, Quantum Design). The Magnetocapacitance can be obtained via the formula $MC = [\varepsilon'(H,T)-\varepsilon'(0,T)]/\varepsilon'(0,T)$, where $\varepsilon'(0,T)$ are dielectric constants of the thin film in the presence and absence of the magnetic field at 10 kHz at room temperature.

3. Results and discussion

Fig. 1 shows the X-ray diffraction (XRD) patterns of the $La_{0.5}Pr_{0.5}FeO_3$ thin films crystallized at 500 °C/2 h in a static environment atmosphere. All diffraction peaks are associated with the $LaFeO_3$ phase (ICSD # 195543) [24] with an orthorhombic perovskite structure and *Pbnm* space group. The Pt(111) substrate characteristic peak was observed at $2\theta = 40°$. No secondary phase peaks were identified, despite the large degree of Pr^{3+}-substitution, which is indicative that the Pr^{3+} ions were successfully incorporated into the La^{3+} sites, forming a complete solid-solution. Table 1 summarizes all structural and Rietveld parameters for the $La_{0.5}Pr_{0.5}FeO_3$ thin film. The Rietveld parameters (χ^2, R_{wp}, and R_{exp}) indicate a coherent fitting of the XRD data [22]. Additionally, the occupancy factor obtained in the Rietveld analysis indicates the incorporation of Pr^{3+} ions at the La^{3+} sites, which may cause the reduction of the unit cell volume [15] due to the difference in the ionic radius of La^{3+} (1.36 Å) and Pr^{3+} (1.13 Å). The volume of the unit cell calculated using Topas V5 (V = 241.16 $Å^3$) corroborates this discussion, as previously reported [24]. The average nanocrystallite size of the orthoferrite phase is approximately 94 nm, with the most pronounced peak (121) located at $2\theta = 32.550°$. Finally, the microstrain values (Table 1) calculated for both the $La_{0.5}Pr_{0.5}FeO_3$ and platinum phases indicate a higher mechanical stress at the Pt substrate which may result in the slight peak shift and broadening that is observed.

Fig. 2 shows the Raman spectrum collected at room temperature for the $La_{0.5}Pr_{0.5}FeO_3$ thin films between 100 and 900 cm^{-1}. Symmetry deviations caused by distortions, breathing, and tilting of the FeO_6 clusters, linked by strong O–Fe–O bonds, and whose internal vibration spectra can provide valuable information on local (short) order-disorder. Group theory predicts 24 possible Raman active vibrational modes among 60 zone-center (Γ-point) phonon modes in the Pbnm structure (Γ-point: 7 A_{1g} + 7 B_{1g} + 5 B_{2g} + 5 B_{3g}) [24,25]. Experimentally, 13 modes were identified in the Raman spectrum (6 A_{1g} + 3 B_{1g} + 1 B_{2g} + 1 B_{3g}) according to the literature [24,26,27], and two which had not been previously reported. The main vibrational modes identified in the Raman spectra are listed in Table 2. The modes located at 120 (B_{1g}) and 192 (A_{1g}) cm^{-1} indicate La/Pr – stretching vibrations. Bending/breathing vibrations in the FeO_6 octahedra can be ascribed to the A_{1g} modes located at 227, 267, and 325 cm^{-1}, respectively. The mode A_{1g}, at 357 cm^{-1} is associated with rotation/bending of the FeO_6 octahedra. The B_{1g} mode located at 420 cm^{-1} can be related to the rotation/stretching of the FeO_6 octahedra. O–Fe–O rotation/bending vibrations are ascribed to the B_{1g} mode at 478 cm^{-1}. Finally, the phononic modes located at 536 (A_{1g}), 617 (B_{1g}), and 660–730 (A_{1g}) cm^{-1} correspond to the asymmetric stretching of Fe–O bonds in the FeO_6 octahedra, which can be associated with the Jahn–Teller distortion [26]. The incorporation of a smaller ion (Pr^{3+}) at the La-sites distorts the structure [28]. Since Pr^{3+} ions (1.13 Å) are markedly smaller than the La^{3+} ion (1.36 Å), the Pr^{3+} bonds that replace La^{3+} in the orthoferrite cluster with the surrounding O^{2-} ions are bigger than the same bonds in the orthoferrite crystal. It is worth highlighting that the introduction of a lighter species leads to a compression of the lattice, affecting the La–O and Fe–O Raman modes. It is important to point out that results obtained using Raman spectroscopy are consistent with those obtained by XRD.

The FEG-SEM image of the $La_{0.5}Pr_{0.5}FeO_3$ thin film (Fig. 3) shows it to be crack-free and has a homogeneous microstructure, with grains of about 70–85 nm, which are compatible with those seen in the XRD analysis (~90 nm). Grain size analysis is essential since it directly affects the thin film's properties, such as magneto coupling, resistive switching behavior, dielectric permittivity, domain arrangements, imprint, among others. For instance, the magnetic properties of $La_{0.5}Pr_{0.5}FeO_3$ are improved as particle size decreases due to the finite-size effect. The preparation method and doping can decrease the size and enhance the values of the coercive field, magnetization, and remnant magnetization [29,30]. Moreover, the shape of the particles has also been proven to influence its properties [31]. In general, grain sizes are randomly distributed with

Table 1
Crystal structure data and refinement results for the $La_{0.5}Pr_{0.5}FeO_3$ thin films deposited on Pt/Ti/SiO_2/Si(100) substrates and annealed at 500 °C for 2 h.

$La_{0.5}Pr_{0.5}FeO_3$ film							
phase (%)	a (Å)	b (Å)	c (Å)	Microstrain	R_{Bragg}	Occ. La^{3+}	Occ. Pr^{3+}
100.0	5.54	5.56	7.83	0.0017(8)	1.47	0.69	0.31
	Pt substrate						
a (Å)		Microstrain				R_{Bragg}	
3.81		0.0018(3)				2.49	
Rietveld parameters							
R_{exp}		R_{wp}		R_p		χ^2	
4.81		7.42		5.00		1.54	

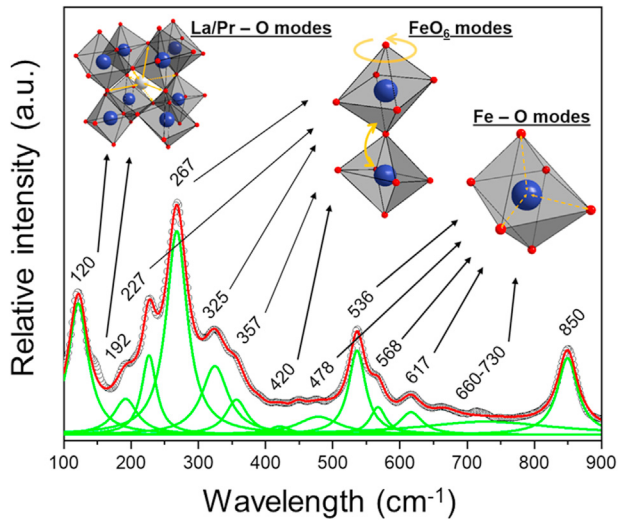

Fig. 2. Raman spectroscopy of the $La_{0.5}Pr_{0.5}FeO_3$ thin films deposited on Pt/Ti/SiO_2/Si(100) substrates and annealed at 500 °C for 2 h.

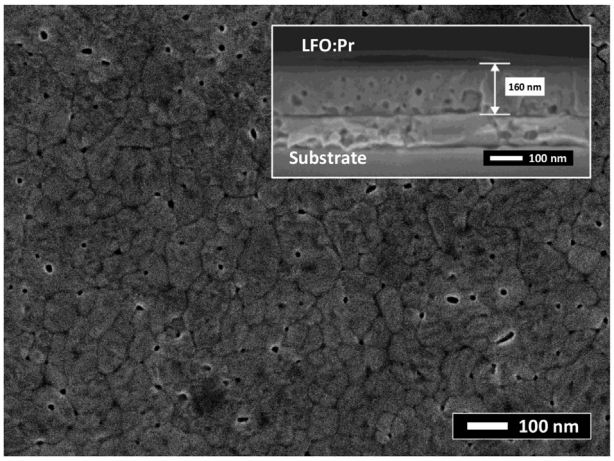

Fig. 3. FEG-SEM and cross-section (inset) images of the $La_{0.5}Pr_{0.5}FeO_3$ thin films deposited on Pt/Ti/SiO_2/Si(100) substrates and annealed at 500 °C for 2 h.

spherical morphology. The cross-sectional view (inset in Fig. 3) shows that the thickness of the thin film is 160 nm. The surface morphology is smooth, indicating that the precursor resin provokes and optimizes the nucleation and growth process of the crystalline phase.

The hysteresis loop for the film measured at room temperature is represented in Fig. 4a. The film tends to saturation with a 2.5 kV/cm electric field. Since the films are polycrystalline, no greater polarization is expected. Besides that, due to the fine-grain microstructure (70–85 nm), a moderate coercive field is noted, considering that the films with small grains present a lessened polarization switching phenomena. At 60 Hz, no contribution of leakage current was detected. The absence of imprint phenomenon was also confirmed, which indicates no displacement along the coercive field axis towards the positive direction. This type of defect can damage the capacitor due to the apparent polarization loss in one of the reminiscent states caused by the voltage fluctuation. Consequently, the coercive field can increase in one direction leading to capacitor memory failure. No traces of space charges coming from trapped (O_2) attached to other electronic defects such as oxygen vacancies (V_O) or dipole complexes associated with iron vacancies (V''_{Fe}-$V^{\bullet\bullet}_O$) are evident in such film. It can be assumed that the conduction mechanism of the orthoferrites comes from the fact that electrons hopped from Fe^{2+} to Fe^{3+} when ($V^{\bullet\bullet}_O$) are present in the film, acting as a "bridge" between iron ions 2+ or 3+ oxidation states. Therefore, as the shape of our hysteresis is symmetric, we

Table 2
Raman mode assignment for the $La_{0.5}Pr_{0.5}FeO_3$ thin films deposited on Pt/Ti/SiO_2/Si(100) substrates and annealed at 500 °C for 2 h.

Symmetry	Mode ±1 (cm^{-1})	Ref. (cm^{-1}) [19,21,22]	Atomic motion description
B_{1g}	120	106	La/Pr–O stretching
A_{1g}	192	185	La/Pr–O stretching
A_{1g}	227	219	FeO_6 bending/breathing
A_{1g}	267	271	FeO_6 bending/breathing
A_{1g}	325	–	FeO_6 bending/breathing
A_{1g}	357	342	FeO_6 rotation/bending
B_{1g}	420	433	FeO_6 rotation/stretching
B_{1g}	478	493	O–Fe – O rotation/bending
A_{1g}	536	557	Fe–O asymetric stretching/breathing
B_{1g}	617	627	Fe–O asymetric stretching/breathing
A_{1g}	660–730	–	Fe–O asymetric stretching/breathing
–	850	–	Not previously reported

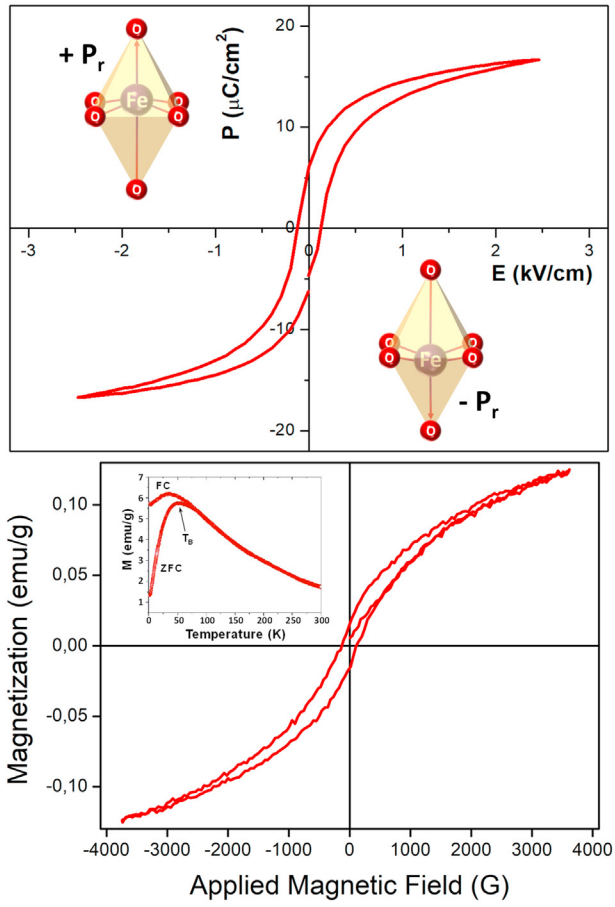

Fig. 4. Field dependencies of the polarization and magnetization obtained for the $La_{0.5}Pr_{0.5}FeO_3$ thin films deposited on $Pt/Ti/SiO_2/Si(100)$ substrates and annealed at 500 °C for 2 h. The inset shows the FC and ZFC curves for the same film.

can assume that the film-electrode interface contains a small concentration of space charges. Saturation polarization (P_s), remnant polarization (P_r), and the electric coercivity (E_c) values (Table 3) for the thin film were obtained via the ferroelectric hysteresis loop in Fig. 4a. The magnetic hysteresis (M-H loop) obtained for $La_{0.5}Pr_{0.5}FeO_3$ thin films indicates the presence of magnetic ordering due to its non-linear behavior, as shown in Fig. 4b. The maximum applied field for the AC loop was ~3600 G, and the loop did not reach saturation. Usually, this phenomenon occurs due to the asymmetric distribution of oxygen vacancies caused by the internal field affecting the alignment of complex dipoles. Besides that, such positively charged oxygen vacancies (V_O) near the negative electrode holds the electrons close to the positive electrode. Consequently, the strong super-exchange interaction generates antiferromagnetic alignment of the iron ions (Fe^{3+}) spins, since the Fe^{3+}-O^{2-}-Fe^{3+} angle is 180° [32]. In orthoferrites, iron ions occupy the distorted octahedral site, and this distortion causes the octahedron to tilt toward the c-axis. In this analysis, the magnetization increases linearly as the applied magnetic field raises, which inhibits the presence of dominant paramagnetic particles. The nonlinear curve is characteristic of the ferri/ferromagnetic variation, where magnetization slowly approaches saturation. Typically, $LaFeO_3$ shows paramagnetic behavior at room temperature. This slightly ferromagnetic behavior is associated with coupling between cations at the octahedral and tetrahedral sites. From this, it can be suggested that the ratio $S = M_r/M_s$ can be used as an important functional parameter to evaluate the magnetic domain

Table 3
Ferroelectric parameters for the $La_{0.5}Pr_{0.5}FeO_3$ thin films deposited on $Pt/Ti/SiO_2/Si(100)$ substrates and annealed at 500 °C for 2 h.

Ferroelectric property	Values
Saturation polarization (P_s)	16.59 ± 0.06 μC/cm²
Remnant polarization (P_r)	6.08 ± 0.11 μC/cm²
Electric coercivity (E_c)	0.125 ± 0.004 kV/cm

boundaries of powdered nanomaterials. This is why our polymeric precursor method can have various domain sizes, and H_c, M_r, and S will be nonzero. Since the coercive field differs from zero and the open hysteresis loop is in conjunction with the high magnetization, the ferromagnetic transition temperature is expected to be greater than the ambient temperature. A remnant magnetization of 12.3 emu/g was measured and can be attributed to three magnetic interactions (Pr—Pr, Pr—Fe, Fe—Fe). However, in LFO, only Fe—Fe interactions contribute to magnetization. This magnetization originates from uncompensated antiferromagnetism resulting from the canting of Fe^{3+} moments. The introduction of Pr^{3+} ions in the La^{3+} lattice sites causes the hysteresis to take on a butterfly shape. Changes in the hysteresis shape can be induced by variations in the crystallite form and/or size, not to mention structural modifications such as the length and angle of Fe—O—Fe bonds and tilting of the (FeO_6) octahedra due to the decrease in the A site radius. The ZFC and FC curves are illustrated as an inset in Fig. 4b. The blocking temperature (T_B) at ~51 K is evidenced by the ZFC curve, and above such temperature, the magnetization vanishes as the temperature decreases, indicating a surface spin-glass transition of antiferromagnetic systems [33–35]. The movement of domain walls allows the bifurcation of the thermal variation of magnetization measured in the ZFC and the FC curves. Since the sample presents spontaneous polarization, it is reasonable to assume a ferroelectric ordering of dipole moment configuration. Therefore, the thin films prepared by the PPM method presents both magnetic and ferroelectric orderings. According to Morozovska et al. [13], the size effects of semi-ellipsoidal $BiFeO_3$ nanoparticles clamped to a rigid conductive substrate can be calculated in the framework of the modified Landau-Ginzburg Devonshire (LGD) approach. The authors mention that the size effect on the phase diagrams, spontaneous polarization, and paramagnetoelectric coefficient is rather sensitive to the aspect ratio of particle sizes in the polarization direction, $bc = a^2$, and less sensitive to the absolute values of the sizes. Assuming that $La_{0.5}Pr_{0.5}FeO_3$ thin films obtained by the polymeric precursor method present grain sizes ranging from 70 to 85 nm, then distinct sources of stress can be presented due to the surface tension itself, as well as from regions enriched by e.g. oxygen vacancies and/or other planar defects. However, the contributions of each effect are additive and therefore more advanced studies should be performed to understand the role of size effects in the multiferroic properties of the orthoferrite film. To do that, films with distinct grain sizes should be grown and the spontaneous polarization dependence, linear dielectric susceptibility, and paramagnetoelectric coefficient should be determined. Furthermore, as the quantitative phase analysis has shown no impurities, no significant effect on the magnetic transition temperature of the film should be considered. As reported by the same authors, the presence of impurities can alter the magnetic transition temperature due to the contribution of the rotomagnetic and magnetostriction coupling. The presence of these couplings can be much more pronounced in $BiFeO_3$ dense fine-grained ceramics due to the internal intergranular stresses. In the case of thin films, Raman modes for different film thickness should be considered and the role of the tilting, rotation, stretching, and breathing of FeO_6 better understood in the rotomagnetic and magnetostriction coupling.

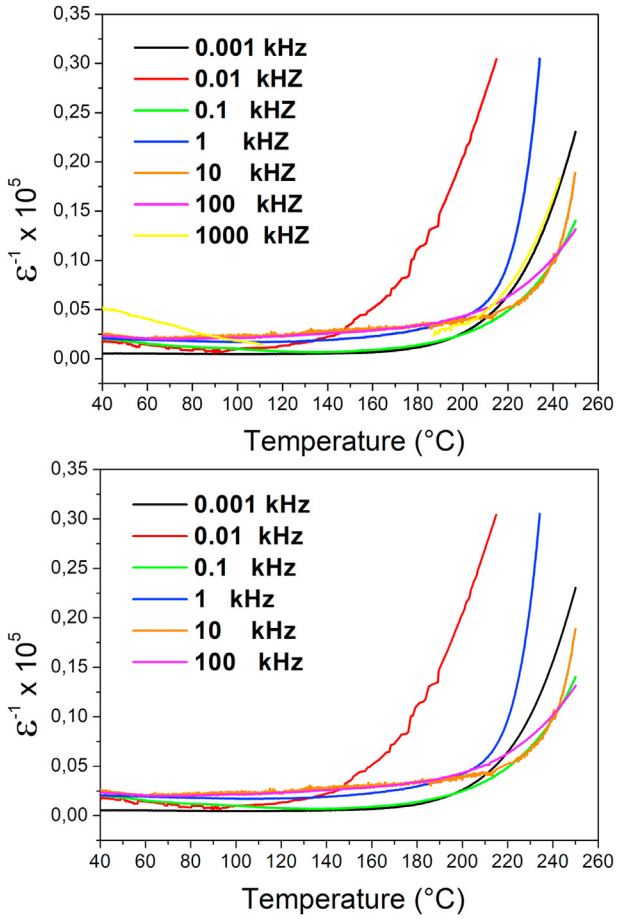

Fig. 5. Thermal variations of ε' and ε'' for the $La_{0.5}Pr_{0.5}FeO_3$ thin films deposited on Pt/Ti/SiO_2/Si(100) substrates and annealed at 500 °C for 2 h.

Fig. 5a and b illustrate the dielectric constants and loss tangent (ε' and ε'') for different frequencies as a function of temperature. The thin film shows small dielectric dispersion at low frequencies, indicating a sharp interface between the Pt substrate and the $La_{0.5}Pr_{0.5}FeO_3$ film as well as low space charges located at the substrate/film interface. The low dispersion of the ε' and ε'' and the absence of any relaxation peak in ε'' indicate that the interfacial polarization of the Maxwell Wagner type was not evident in the spectra. As the values of ε' and ε'' at lower temperatures (<330 K) remains constant, no significant effect on the overall morphology of the film takes place [36–39]. So, the high value of ε' and ε'' at elevated temperatures as well as at room temperature may be due to the ferroelectric ordering present in the system as a consequence of the large mismatch between the bottom electrode and the orthoferrite thin film as indicated by microstrain values calculated for the $La_{0.5}Pr_{0.5}FeO_3$ film and Pt substrate using the Rietveld analysis (Table 1) Literature reports that applying a magnetic field creates a magnetic order that affects the dielectric constant of multiferroics [40–43]. To prove that, we can measure the changes in the dielectric constant in the presence and absence of a magnetic field (Fig. 6a). A positive coupling is observed, indicating an increase in ε' with the magnetic field (H), with the maximum value of magneto coupling around 0.06 for H ~1.7 T. Also, due the coupling between the ferroelectric and magnetic domains, the strain will induce stress which generates an electric field on the ferroelectric domains as well as in the presence of H, the multiferroic film is strained [44]. Accordingly, Fig. 6b illustrates a compilation of the effects in the $La_{0.5}Pr_{0.5}FeO_3$ orthoferrite structure that leads to the magnetoelectric coupling phenomena. As mentioned before, modifications in the length and angle of the Fe–O–Fe bonds and tilting of the oxygen octahedra influence the magnetic and ferroelectric properties. The distorted FeO_6 octahedral sites are characterized by the rotations of these atomic groups with respect to the cubic A_8 (A = La, Pr) cells in the lattice, which can be defined by the tilt angle, as shown in Fig. 6b. The lattice distortion introduced by both FeO_6 tilting and dopant cations creates a local electric field responsible for the ferroelectric ordering in $La_{0.5}Pr_{0.5}FeO_3$. The presence of these oxygen octahedra distortions are evidenced by the Raman modes attributed to the tilting, rotation, stretching, and breathing of FeO_6 in Fig. 2. Moreover, the rotation of the oxygen octahedra is characteristic of antiferrodistorted perovskites, and the coupling between the tilt angle and the antiferromagnetic order (rotomagnetic coupling) is very important to describe their properties, as reported in the literature [14,45].

Considering the conduction mechanism of the $La_{0.5}Pr_{0.5}FeO_3$ originates from the fact that electrons are hopped from Fe^{2+} to Fe^{3+}, we employed XPS spectroscopy (Fig. 7) to provide greater insight on the processes occurring on the surface. The evolution of the structural components was analyzed by the deconvolution of the Fe $2p_{3/2}$ and Fe $2p_{1/2}$ spectra, providing information on the spin-orbit doublet components of the Fe 2*p* photoemission. Fe^{2+} and Fe^{3+} components were located at 712.2 and 725.6 eV, with no traces of metallic Fe. This indicates the simultaneous presence of Fe^{2+} and Fe^{3+} ions in the thin film, which is consistent with electrical measurements. The surface plays an important role in both the electromagnetic response of $La_{0.5}Pr_{0.5}FeO_3$ based films especially in thin films, in which the surface-to-volume ratio increases considerably over the bulk materials. In orthoferrites**,** the electromagnetic properties may be explained based on hopping conduction, which may be associated with structural distortions of the MO_6 octahedra. The formation of mono-ionized oxygen vacancies is seen through XPS analysis, which shows simultaneous presence of Fe^{2+} and Fe^{3+} ions in the films, and corroborates the electrical measurements. Such results are advantageous for producing orthoferrites materials with low leakage and positive coupling caused by an increase in ε' with the magnetic field (H). The thin film indicate**s** a pure phase with no traces of other spin-orbit component, hinting at the formation of a single perovskite phase detected on the surface.

The typical hysteresis curve observed in the picture for the $La_{0.5}Pr_{0.5}FeO_3$ film reveals a clockwise rotation characteristic of dielectric films, as shown in Fig. 8. The existence of Fe^{2+} and Fe^{3+} ions with oxygen vacancies in the lattice promotes electron hopping, in turn leading to such behavior. As the film was deposited on a p-type Pt substrate, by applying a voltage in the opposite direction leads to charge accumulation at negative bias voltages, this suggests that a depletion layer was formed inside the Pt substrate near the interface. The *I–V* curve is almost symmetrical, implying that an increase in voltage caused an inversion of the surface and that no significant difference was observed when the bias was reversed. For nonvolatile memory operation, the desired switching mode occurs when the charge compensation on the surface is induced by the polarization present in the film. We observe that the difference in the resistance modulation arises mainly from the magnitude of the high-resistance OFF-state, the resistance in the ON-state. The $La_{0.5}Pr_{0.5}FeO_3$ film took 18.0 V and −28.12 V for SET and RESET processes, respectively, as well as a lower power consumption due to the extremely reduced current, below 1.0 μA. The small current value requires less energy to perform due to the lower necessary voltages. Therefore, the results obtained in this study are auspicious regarding $La_{0.5}Pr_{0.5}FeO_3$ thin-film applications on RRAM devices, due to the low energy consumption and dimensions on the

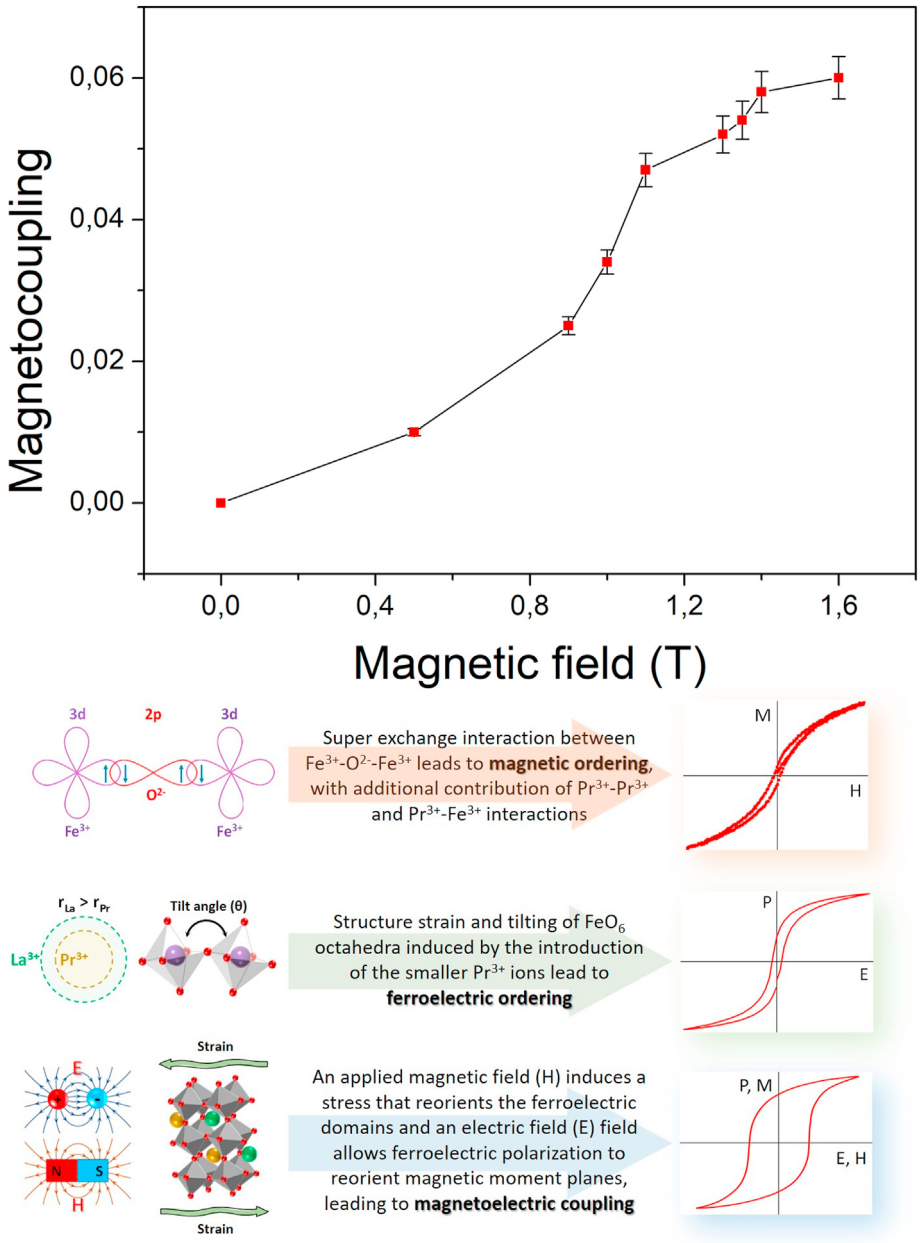

Fig. 6. Magneto-coupling as a function of the magnetic field (a) for the $La_{0.5}Pr_{0.5}FeO_3$ thin films deposited on Pt/Ti/SiO_2/Si(100) substrates and annealed at 500 °C for 2 h (the line connecting the points is used to guide the eyes) and (b) illustration of the magnetoelectric coupling in the $La_{0.5}Pr_{0.5}FeO_3$ orthoferrite.

nanoscale, two of the most critical requirements for the development of future electronic devices.

4. Conclusions

The multiferroic compound $La_{0.5}Pr_{0.5}FeO_3$ was chemically synthesized using the polymeric precursor method. The crystallographic phase was identified by XRD data, and with no impurities. At room temperature, a typical ferroelectric loop suggests a new multiferroic system, where the coexistence of coupled magnetic and ferroelectric orderings was observed. The M-H behavior originated from the uncompensated antiferromagnetic character from the canting of Fe^{3+} moments. Dielectric measurements reveal low dispersion of the ε' and ε'', while the absence of any relaxation peak in ε'' indicate**s** that the interfacial polarization of the Maxwell Wagner type was neglected. The ZFC curve reveals a blocking temperature (T_B) at ~51 K and a reduction of magnetization as the temperature decreases, indicating a surface spin-glass transition of antiferromagnetic systems. The positive magnetoelectric coupling obtained reveal**s** an increase in ε' with the magnetic field (H) due the modifications in the length and angle of Fe—O—Fe bonds and tilting of the oxygen octahedra. This hypothesis is supported by oxygen octahedra distortions evidenced by the Raman modes attributed to the tilting, rotation, stretching, and breathing of FeO_6. The coupling between the tilt angle and the antiferromagnetic order (rotomagnetic coupling) in antiferrodistorted perovskites could be caused by the rotation of the oxygen octahedra as demonstrated by Raman spectra. The I—V hysteresis curve reveals a clockwise rotation, requiring 18.0 V and - 28.12 V for SET/RESET modes, respectively, along with lower power consumption due to the

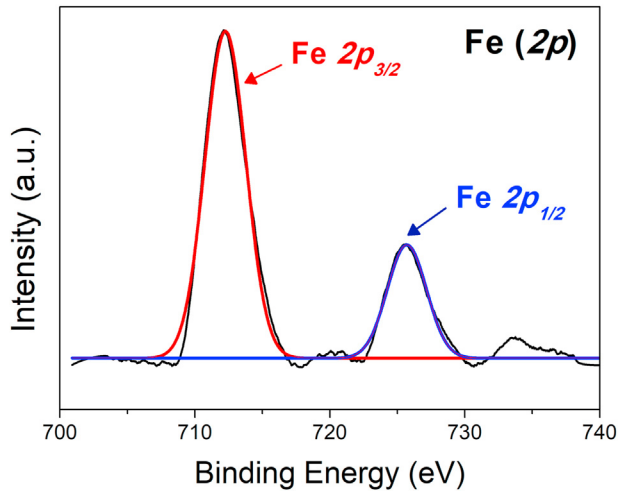

Fig. 7. XPS spectra for $La_{0.5}Pr_{0.5}FeO_3$ thin film showing spin orbit doublets of Fe $2p_{3/2}$ and Fe $2p_{1/2}$.

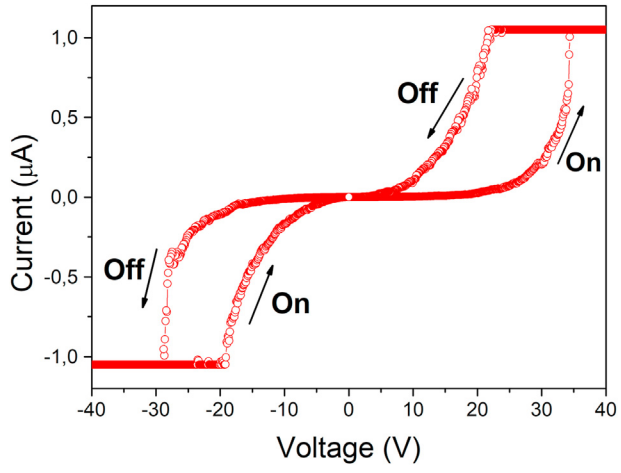

Fig. 8. I–V curves on the SET/RESET modes of the $La_{0.5}Pr_{0.5}FeO_3$ thin films deposited on Pt/Ti/SiO_2/Si(100) substrates and annealed at 500 °C for 2 h.

extremely reduced current, below 1.0 μA. These several aspects are interesting for $La_{0.5}Pr_{0.5}Fe0_3$, which is a novel multiferroic material recommended for spintronic applications.

CRediT authorship contribution statement

M.G.A. Ranieri: Conceptualization, Methodology. **P.P. Ortega:** Original Draft Preparation, Formal analysis. **H. Moreno:** Formal analysis, Review & Editing. **M.A. Ramirez:** Formal analysis, Review & Editing. **E.C. Aguiar:** Investigation. **A.Z. Simões:** Conceptualization, Methodology, Supervision.

Declaration of competing interest

The authors declare that they have no known competing financial interests or personal relationships that could have appeared to influence the work reported in this paper.

Acknowledgments

The authors gratefully acknowledge the financial support of the Sao Paulo State Research Foundation (FAPESP) and CDMF (Functional Materials Development Center), process number 2013/07296–2. We would like to thank Manuel da Silva for the magnetic measurements.

References

[1] L. Hou, L. Shi, J. Zhao, S. Zhou, S. Pan, X. Yuan, Y. Xin, Room-temperature multiferroicity in $CeFeO_3$ ceramics, J. Alloys Compd. 797 (2019) 363–369, https://doi.org/10.1016/j.jallcom.2019.05.078.
[2] N.A. Spaldin, R. Ramesh, Advances in magnetoelectric multiferroics, Nat. Mater. 18 (2019) 203–212, https://doi.org/10.1038/s41563-018-0275-2.
[3] S. Kumar Arti, P. Kumar, R. Walia, V. Verma, Improved ferroelectric, magnetic and photovoltaic properties of Pr doped multiferroic bismuth ferrites for photovoltaic application, Results Phys 14 (2019) 102403, https://doi.org/10.1016/j.rinp.2019.102403.
[4] P.P. Ortega, L.S.R. Rocha, C.C. Silva, M. Cilense, R.A.C. Amoresi, E. Longo, A.Z. Simões, Multiferroic behavior of heterostructures composed of lanthanum and bismuth ferrite, Ceram. Int. 42 (2016) 16521–16528, https://doi.org/10.1016/j.ceramint.2016.07.070.
[5] K. Wang, N. Si, Y.L. Zhang, F. Zhang, A.B. Guo, W. Jiang, First-principles study on magnetoelectric coupling effect of M/$BiFeO_3$ (M = Co, Fe) multiferroic superlattice, Vacuum 165 (2019) 105–112, https://doi.org/10.1016/j.vacuum.2019.04.009.
[6] R. Souza, The "holy grail" of multiferroic physics, Phys. Can. 72 (2016) 57–62.
[7] R. Ramesh, N.A. Spaldin, Multiferroics: progress and prospects in thin films, Nat. Mater. 6 (2007) 21–29, https://doi.org/10.1038/nmat1805.
[8] S. Acharya, J. Mondal, S. Ghosh, S.K. Roy, P.K. Chakrabarti, Multiferroic behavior of lanthanum orthoferrite ($LaFeO_3$), Mater. Lett. 64 (2010) 415–418, https://doi.org/10.1016/j.matlet.2009.11.037.
[9] S. Mallesh, J. Krishnamurthy, A.K. Das, A. Venimadhav, D. Chandrasekhar Kakarla, Anomalous freezing of dielectric polarons near magnetic ordering in multiferroic $La_{0.5}Bi_{0.5}FeO_3$, Ceram. Int. 45 (2019) 6250–6254, https://doi.org/10.1016/j.ceramint.2018.12.105.
[10] A. Mitra, A.S. Mahapatra, A. Mallick, P.K. Chakrabarti, Enhanced microwave absorption and magnetic phase transitions of nanoparticles of multiferroic $LaFeO_3$ incorporated in multiwalled carbon nanotubes (MWCNTs), J. Magn. Magn Mater. 435 (2017) 117–125, https://doi.org/10.1016/j.jmmm.2017.03.066.
[11] A. Mitra, A.S. Mahapatra, A. Mallick, A. Shaw, N. Bhakta, P.K. Chakrabarti, Improved magneto-electric properties of $LaFeO_3$ in $La_{0.8}Gd_{0.2}Fe_{0.97}Nb_{0.03}O_3$, Ceram. Int. 44 (2018) 4442–4449, https://doi.org/10.1016/j.ceramint.2017.12.045.
[12] E.A. Eliseev, M.D. Glinchuk, V. Gopalan, A.N. Morozovska, Rotomagnetic couplings influence on the magnetic properties of antiferrodistortive antiferromagnets, J. Appl. Phys. 118 (2015) 144101, https://doi.org/10.1063/1.4932211.
[13] A.N. Morozovska, E.A. Eliseev, M.D. Glinchuk, O.M. Fesenko, V.V. Shvartsman, V. Gopalan, M.V. Silibin, D.V. Karpinsky, Rotomagnetic coupling in fine-grained multiferroic $BiFeO_3$: theory and experiment, Phys. Rev. B 97 (2018) 134115, https://doi.org/10.1103/PhysRevB.97.134115.
[14] D.V. Karpinsky, E.A. Eliseev, F. Xue, M.V. Silibin, A. Franz, M.D. Glinchuk, I.O. Troyanchuk, S.A. Gavrilov, V. Gopalan, L.Q. Chen, A.N. Morozovska, Thermodynamic potential and phase diagram for multiferroic bismuth ferrite ($BiFeO_3$), NPJ Comput. Mater. 3 (2017) 20, https://doi.org/10.1038/s41524-017-0021-3.
[15] E. Folven, T. Tybell, A. Scholl, A. Young, S.T. Retterer, Y. Takamura, J.K. Grepstad, Antiferromagnetic domain reconfiguration in embedded $LaFeO_3$ thin film nanostructures, Nano Lett. 10 (2010) 4578–4583, https://doi.org/10.1021/nl1025908.
[16] A. Mitra, A.S. Mahapatra, A. Mallick, A. Shaw, M. Ghosh, P.K. Chakrabarti, Simultaneous enhancement of magnetic and ferroelectric properties of $LaFeO_3$ by co-doping with Dy^{3+} and Ti^{4+}, J. Alloys Compd. 726 (2017) 1195–1204, https://doi.org/10.1016/j.jallcom.2017.08.074.
[17] P. Noël, F. Trier, L.M. Vicente Arche, J. Bréhin, D.C. Vaz, V. Garcia, S. Fusil, A. Barthélémy, L. Vila, M. Bibes, J.P. Attané, Non-volatile electric control of spin–charge conversion in a $SrTiO_3$ Rashba system, Nature 580 (2020) 483–486, https://doi.org/10.1038/s41586-020-2197-9.
[18] J.A. Mundy, C.M. Brooks, M.E. Holtz, J.A. Moyer, H. Das, A.F. Rébola, J.T. Heron, J.D. Clarkson, S.M. Disseler, Z. Liu, A. Farhan, R. Held, R. Hovden, E. Padgett, Q. Mao, H. Paik, R. Misra, L.F. Kourkoutis, E. Arenholz, A. Scholl, J.A. Borchers, W.D. Ratcliff, R. Ramesh, C.J. Fennie, P. Schiffer, D.A. Muller, D.G. Schlom, Atomically engineered ferroic layers yield a room-temperature magnetoelectric multiferroic, Nature 537 (2016) 523–527, https://doi.org/10.1038/nature19343.
[19] M.G.A. Ranieri, M. Cilense, E.C. Aguiar, A.Z. Simões, M.A. Ponce, E. Longo, $La_{0.5}Sm_{0.5}FeO_3$: a new candidate for magneto-electric coupling at room temperature, J. Mater. Sci. Mater. Electron. 28 (2017) 10747–10757, https://doi.org/10.1007/s10854-017-6851-4.
[20] M.G.A. Ranieri, M. Cilense, E.C. Aguiar, C.C. Silva, A.Z. Simões, E. Longo, Electrical behavior of chemically grown lanthanum ferrite thin films, Ceram. Int. 42 (2016) 2234–2240, https://doi.org/10.1016/j.ceramint.2015.10.016.
[21] A.Z. Simões, A.H.M. González, M.A. Zaghete, J.A. Varela, B.D. Stojanovic, Effects of annealing on the crystallization and roughness of PLZT thin films, Thin Solid Films 384 (2001) 132–137, https://doi.org/10.1016/S0040-6090(00)01782-X.

[22] A.A. Coelho, TOPAS and TOPAS-Academic: an optimization program integrating computer algebra and crystallographic objects written in C++: an, J. Appl. Crystallogr. 51 (2018) 210–218, https://doi.org/10.1107/S1600576718000183.
[23] H.M. Rietveld, A profile refinement method for nuclear and magnetic structures, J. Appl. Crystallogr. 2 (1969) 65–71, https://doi.org/10.1107/s0021889869006558.
[24] S. Chanda, S. Saha, A. Dutta, B. Irfan, R. Chatterjee, T.P. Sinha, Magnetic and dielectric properties of orthoferrites La_{1-x} Pr_xFeO_3 (x = 0, 0.1, 0.2, 0.3, 0.4 and 0.5), J. Alloys Compd. 649 (2015) 1260–1266, https://doi.org/10.1016/J.JALLCOM.2015.07.215.
[25] M.K. Singh, H.M. Jang, H.C. Gupta, R.S. Katiyar, Polarized Raman scattering and lattice eigenmodes of antiferromagnetic $NdFeO_3$, J. Raman Spectrosc. 39 (2008) 842–848, https://doi.org/10.1002/jrs.
[26] M. Popa, L. Van Hong, M. Kakihana, Nanopowders of $LaMeO_3$ perovskites obtained by a solution-based ceramic processing technique, Phys. B Condens. Matter 327 (2003) 233–236, https://doi.org/10.1016/S0921-4526(02)01736-2.
[27] P.V. Coutinho, F. Cunha, P. Barrozo, Structural, vibrational and magnetic properties of the orthoferrites $LaFeO_3$ and $YFeO_3$: a comparative study, Solid State Commun. 252 (2017) 59–63, https://doi.org/10.1016/j.ssc.2017.01.019.
[28] A. Rai, A.K. Thakur, Influence of co-substitution driven property tailoring in lanthanum orthoferrites ($LaFeO_3$), Ceram. Int. 43 (2017) 13828–13838, https://doi.org/10.1016/j.ceramint.2017.07.103. https://search.crossref.org/?q=Influence+of+co-substitution+driven+property+tailoring+in+lanthanum+orthoferrites+%28LaFeO3%29.
[29] S. Phokha, S. Hunpratup, S. Pinitsoontorn, B. Putasaeng, S. Rujirawat, S. Maensiri, Structure, magnetic, and dielectric properties of Ti-doped $LaFeO_3$ ceramics synthesized by polymer pyrolysis method, Mater. Res. Bull. 67 (2015) 118–125, https://doi.org/10.1016/j.materresbull.2015.03.008.
[30] S. Katba, S. Jethva, M. Vagadia, A. Ravalia, D.G. Kuberkar, Effect of La-substitution on magnetic properties of $ErFeO_3$ orthoferrites, J. Magn. Magn Mater. 514 (2020), https://doi.org/10.1016/j.jmmm.2020.167170.
[31] V.V. Khist, E.A. Eliseev, M.D. Glinchuk, M.V. Silibin, D.V. Karpinsky, A.N. Morozovska, Size effects of ferroelectric and magnetoelectric properties of semi-ellipsoidal bismuth ferrite nanoparticles, J. Alloys Compd. 714 (2017) 303–310, https://doi.org/10.1016/j.jallcom.2017.04.201.
[32] K. Mukhopadhyay, A.S. Mahapatra, P.K. Chakrabarti, Enhanced magnetoelectric property and exchange bias effect of Zn substituted $LaFeO_3$ ($La_{0.50}Zn_{0.50}FeO_3$), Mater. Lett. 159 (2015) 9–11, https://doi.org/10.1016/j.matlet.2015.06.059.
[33] M. Gitterman, M.W. Klein, Spin-glass transition in a system with competing ferromagnetic and antiferromagnetic interaction, Phys. Rev. B 14 (1976) 4224–4226, https://doi.org/10.1103/PhysRevB.14.4224.
[34] A. Indra, S. Giri, Multiferroic order and re-entrant spin-glass-like state in $DyCrO_4$, J. Magn. Magn Mater. 489 (2019) 165467, https://doi.org/10.1016/j.jmmm.2019.165467.
[35] H. Wang, C. Dong, Z. Li, J. Yang, Q. Mao, M. Fang, Evolution from antiferromagnetic order to spin-glass state in $Fe_{1.05-x}Cu_xTe$ system, Phys. Lett. Sect. A Gen. At. Solid State Phys. 376 (2012) 3645–3648, https://doi.org/10.1016/j.physleta.2012.10.028.
[36] R.S. Devan, S.B. Deshpande, B.K. Chougule, Ferroelectric and ferromagnetic properties of $(x)BaTiO_3+(1-x)Ni_{0.94}Co_{0.01}Cu_{0.05}Fe_2O_4$ composite, J. Phys. D Appl. Phys. 40 (2007) 1864–1868, https://doi.org/10.1088/0022-3727/40/7/004.
[37] A. Haug, Theoretical Solid State Physics, first ed., Pergamon Press, 1972 https://doi.org/10.1016/C2013-0-02343-2.
[38] B.I. Bleaney, B. Bleaney, Electricity and Magnetism, third ed., Oxford University Press, 1994.
[39] C.G. Koops, On the dispersion of resistivity and dielectric constant of some semiconductors at audiofrequencies, Phys. Rev. 83 (1951) 121–124, https://doi.org/10.1103/PhysRev.83.121.
[40] Z.H. Sun, B.L. Cheng, S. Dai, L.Z. Cao, Y.L. Zhou, K.J. Jin, Z.H. Chen, G.Z. Yang, Dielectric property studies of multiferroic $GaFeO_3$, J. Phys. D Appl. Phys. 39 (2006) 2481–2484, https://doi.org/10.1088/0022-3727/39/12/001.
[41] A. Panda, R. Govindaraj, G. Amarendra, Magneto dielectric coupling in $Bi_2Fe_4O_9$, Phys. B Condens. Matter 570 (2019) 206–208, https://doi.org/10.1016/j.physb.2019.06.045.
[42] D. Zhang, J. Cheng, J. Chai, J. Deng, R. Ren, Y. Su, H. Wang, C. Ma, C.S. Lee, W. Zhang, G.P. Zheng, M. Cao, Magnetic-field-induced dielectric behaviors and magneto-electrical coupling of multiferroic compounds containing cobalt ferrite/barium calcium titanate composite fibers, J. Alloys Compd. 740 (2018) 1067–1076, https://doi.org/10.1016/j.jallcom.2018.01.081.
[43] Y. Fang, L.Y. Wang, Y.Q. Song, T. Tang, D.H. Wang, Y.W. Du, Manipulation of magnetic field on dielectric constant and electric polarization in Cr_2WO_6, Appl. Phys. Lett. 104 (2014) 132908, https://doi.org/10.1063/1.4870518.
[44] N.A. Spaldin, Multiferroics beyond electric-field control of magnetism, Proc. R. Soc. A Math. Phys. Eng. Sci. 476 (2020), https://doi.org/10.1098/rspa.2019.0542.
[45] M.D. Glinchuk, A.N. Morozovska, D.V. Karpinsky, M.V. Silibin, Anomalies of phase diagrams and physical properties of antiferrodistortive perovskite oxides, J. Alloys Compd. 778 (2019) 452–479, https://doi.org/10.1016/j.jallcom.2018.11.015.